AIMS Mathematics, 10(12): 30806–30827.
DOI: 10.3934/math.20251352
Received: 22 October 2025
Revised: 18 December 2025
Accepted: 23 December 2025
Published: 30 December 2025

https://www.aimspress.com/journal/Math

Research article

Soliton wave phenomena of the complex hyperbolic nonlinear Schrödinger equation via emerging WAS-Exp neural network method and qualitative analysis

Waseem Razzaq[1], **Asim Zafar**[1], **Ahmed Al Nuaim**[2,*] **and Naif Almusallam**[2]

[1] Department of Mathematics, COMSATS University Islamabad, Vehari Campus, Pakistan

[2] Department of Management Information Systems, School of Business, King Faisal University, Al-Ahsa 31982, Saudi Arabia

* **Correspondence:** Email: aaalnuaim@kfu.edu.sa.

Abstract: The main goal of this work was to develop the new analytical neural network technique known as WAS-Exp neural network method. A mathematical analytical technique that could produce solitary, hyperbolic, trigonometric, and rational wave structures in a single framework to build accurate solutions. An essential model for explaining nonlinear wave propagation in dispersive media like optical fibers and plasma channels is the complex hyperbolic nonlinear Schrödinger dynamical equation, which we examined in this work. In contrast to its classical version, the model improves capture memory and non locality and anomalous dispersion by introducing hyperbolic dispersion. We execute the newly proposed technique on this model and a variety of analytical solutions are obtained using this procedure. The resultant solutions provided new insights into the dynamics of nonlinear systems and their possible applications in plasma physics, optical communications, and related domains by demonstrating the wave behavior through the 3D and 2D surfaces. Furthermore, machine learning analysis was executed on the obtained solution for examining the wave dynamic behavior of the actual and predicted outcomes. Lastly, we plotted the x-asymptotic, y-asymptotic and t-asymptotic of the gain solutions through the 2D surfaces.

Keywords: complex hyperbolic nonlinear Schrödinger equation; WAS-Exp neural network method; analytical method; neural network; soliton solutions; multilayer perceptron reggressor algorithm; asymptotic analysis
Mathematics Subject Classification: 35A20, 35C08, 35Q55, 37K10

1. Introduction

One of the most crucial mathematical tools for simulating intricate dynamical phenomena in a variety of fields, such as fluid mechanics, plasma physics, optical fiber communications, heat transfer, and nonlinear optics, is the nonlinear partial differential equations (NLPDE). Because of their exceptional capacity to maintain speed and shape over extended distances and during mutual interactions, solitons have a central place among their varied solutions structures. John Scott Russel first noticed a single wave moving unmodified in a canal in 1845, which led to discovery of the soliton phenomena [1]. Later, the theory was formalized by Drazin and Johnson [2], who identified three essential properties of solitons: spatial localization, elastic interactions, and shape preservation. Over the years, numerous mathematical models have been developed to capture such nonlinear wave phenomena, including the sine-Gordon equation [3], the sinh-Gordon equation [4], the Zoomeron equation [5], the Bogoyavlensky-Konopelchenko equation [6], the Boussinesq-Burgers equation [7], the Kairat-II and Kairat-X equations [8], the Burger-Fisher equation [9], the Korteweg-de Vries (KdV) equation [10], the Kadomtsev-Petviashvili equation [11], the generalized Schrödinger equation [12], and the Ginzburg-Landau equation [13].

In this article, we use the complex hyperbolic nonlinear Schrödinger dynamical equation (CHNLSDE) [14].

$$iw_{yy} + \frac{1}{2}(w_{xx} - w_{tt}) + |w|^2 w = 0. \tag{1.1}$$

The complex hyperbolic nonlinear Schrödinger dynamical equation is employed in this work because it accounts for hyperbolic dispersion, allowing a more realistic description of memory effects, nonlocality, and anomalous dispersion in physical media. These features make the CHNLSDE more suitable than the classical nonlinear Schrödinger equation for describing nonlinear wave propagation in optical fibers and plasma channels. Thus, it provides a more accurate framework for analyzing complex wave dynamics in dispersive systems. Apeanti et al. [15] used CHNLSDE to acquire new complex rational, trigonometric and hyperbolic solutions. Correia et al. [16] used CHNLSDE to prove a stability result for both spatial plane waves and spatial standing waves with respect to small H^1 perturbation and many others. Also, Nucci's direct method [17], the lie symmetry analysis [18], the bilinear neural network approach [19], the exponential and Kudryashov method [20], the sine-cosine method [21], and the extended generalized Riccati equation mapping method [22], are some of the analytical techniques that have been used to study CHNLSDE and related systems. These investigations show how the model can accurately depict intricate solitary, periodic and rational wave structures, which has immediate applications in applied physics and nonlinear optics.

Significant advancements have been made in the construction of exact analytical solutions to NLPDEs using sophisticated computational approaches. The advanced $exp(-\psi(\eta))$-expansion strategy [23], is one such technique that has just been presented as a methodical and flexible plan for producing trigonometric, hyperbolic, and rational traveling wave solutions. This technique adds an additional equation to the conventional exp-function approach, making it more comprehensive, which allows for a variety of functional forms based on the values and signs of the parameters. The target NLPDE is converted to an ordinary differential equation by applying an appropriate wave transformation, and the solution is given as a logical combination of the exponential terms in $exp(-\psi(\eta))$. This method has been effectively used to solve a variety of nonlinear models such as the

simplified modified Camassa-Holm (SMCH) model [24], Benjamin Bona Mahony Burger model [25], coupled nonlinear Maccari's system [26], (STO)-Burger equation [27], Kuralay model [28] and many more.

In this paper, we derive new classes of exact solitary wave solutions in the framework by combining the analytical power of the advanced $exp(-\psi(\Upsilon))$ with neural network model with the physical richness of the CHNLSDE. The investigation of the combined impacts of nonlinearity, dispersion on wave dynamics in nonlinear dispersive systems is made possible by this synergy. The found solutions are anticipated to enhance the library of exact solutions accessible to NLPDEs and offer important insights into wave theory, nonlinear optical communications, and ultrashort pulse propagation. In addition to expanding our theocratical knowledge of nonlinear equations, these findings offer useful information for applications in plasma physics, optical communications, and other fields where regulating and forecasting wave behavior is crucial. In addition, machine learning analysis executes on the gain solutions to predict the behavior of the wave dynamical profile. Lastly, we find out the asymptotic behavior of the obtained solutions.

Section 1 introduces the CHNLSDE and its significance in nonlinear wave modeling. Section 2 describes the WAS-Exp neural network approach in general terms. Section 3 presents the exact analytical solutions obtained for the model, while Section 4 provides their graphical representations to illustrate the physical behavior. Section 5 executes machine learning analysis. Section 6 describes the asymptotic behavior. Finally, Section 7 concludes the work by summarizing the main findings and highlighting their potential applications.

2. The WAS-Exp neural network method

We propose a novel technique, termed the WAS-Exp neural network method, which integrates the $e^{-\psi(\Upsilon)}$ [23] with a neural network (NN) [29] architecture to derive exact solutions of nonlinear partial differential equations (nPDEs) of the form:

$$\mathcal{P}(w, w_x, w_t, w_{xx}, w_{xt}, w_{tt}, \dots) = 0, \tag{2.1}$$

where $\mathcal{P}$ is a polynomial involving the function w and its partial derivatives with respect to spatial and temporal variables. To find the exact solutions of Eq (2.1), we introduce the trial function of the neural networks (NNs) model shown in Figure 1. The output of NNs serves as the trial function for the solutions of Eq (2.1), and the trial function of the NNs model is as follows:

Let the output w be defined as

$$w = \sum_{l_n \in \mathcal{L}_n} v_{l_n,w} F_{l_n}(\Upsilon_{l_n}), \tag{2.2}$$

where

- $v_{l_n,w}$ is the weight coefficient from the last hidden layer neuron l_n to the output neuron w,
- F is the activation function,
- $\mathcal{L}_n = \{I_{n-1} + 1, I_{n-1} + 2, \dots, I_n\}$ is the index set of neurons in the n-th (last hidden) layer.

The neural network contains two types of parameters:

- weights $v_{i,j}$,

- bias terms θ_l,

which connect neuron i from the previous layer to neuron j in the next layer.

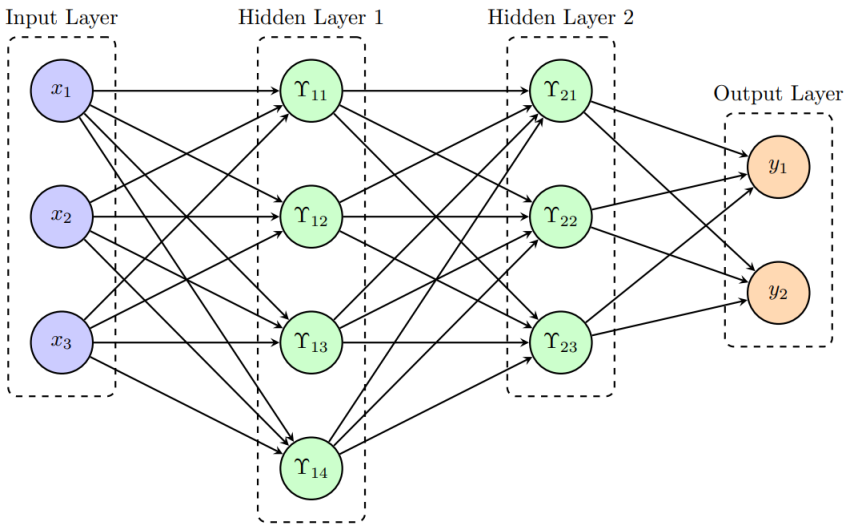

Figure 1. Schematic diagram of the neural network architecture. The input layer receives the independent variables (x_1, x_2, x_3), the hidden layers perform nonlinear feature transformations through the activation functions Υ_{ij} and the output layer produces the predicted solution components (y_1, y_2).

The mathematical expression for Υ_{l_i} in the i-th layer is

$$\Upsilon_{l_i} = \sum_{l_{i-1} \in \mathcal{L}_{i-1}} v_{l_{i-1},l_i} F_{l_{i-1}}(\Upsilon_{l_{i-1}}) + \theta_{l_i}, \quad i = 1, 2, \ldots, n.$$

The WAS-Exp neural network method leverages the analytical properties of the $e^{-\psi(\Upsilon)}$ and the structural flexibility of neural networks.

$$\psi'(\Upsilon) = -(\alpha e^{-\psi(\Upsilon)} + \beta e^{\psi(\Upsilon)}). \tag{2.3}$$

Family 1: Hyperbolic function solutions, when $(\alpha\beta) < 0$,

$$\psi(\Upsilon) = \begin{cases} -\ln\left(\sqrt{\dfrac{\alpha}{-\beta}}\tanh\left(\sqrt{-\alpha\beta}\,(\Upsilon + Q)\right)\right), \\ -\ln\left(\sqrt{\dfrac{\alpha}{-\beta}}\coth\left(\sqrt{-\alpha\beta}\,(\Upsilon + Q)\right)\right). \end{cases} \tag{2.4}$$

Family 2: Solutions for trigonometric functions, when $(\alpha\beta) > 0$,

$$\psi(\Upsilon) = \begin{cases} -\ln\left(\sqrt{\dfrac{\alpha}{\beta}}\tan\left(\sqrt{\alpha\beta}\,(\Upsilon + Q)\right)\right), \\ -\ln\left(-\sqrt{\dfrac{\alpha}{\beta}}\cot\left(\sqrt{\alpha\beta}\,(\Upsilon + Q)\right)\right). \end{cases} \tag{2.5}$$

Family 3: Solutions using rational functions, when $\beta > 0$ and $\alpha = 0$,

$$\psi(\Upsilon) = -\ln\left(\frac{1}{-\beta(\Upsilon + Q)}\right). \tag{2.6}$$

Family 4: When $\beta = 0$ and $\alpha \neq 0$,

$$\psi(\Upsilon) = -\ln\left(\alpha(\Upsilon + Q)\right). \tag{2.7}$$

Here, α, β and Q are the non-zero real constants.

The method functions in two complementary stages:

(1) Embedding known solutions of the $e^{-\psi(\Upsilon)}$ into the neural network as activation functions.
(2) Using the resulting neural network to construct trial functions and transform the nPDE into a solvable algebraic system.

The steps of the WAS-Exp neural network method are as follows:

Step 1. Construct the WAS-Exp NN architecture:

- **Input layer:** Variables such as x, t or higher-dimensional inputs.
- **Hidden layers:** Neurons activated by the $e^{-\psi(\Upsilon)}$ based functions.
- **Output layer:** The trial function $w(x, t)$.

Step 2. Use forward propagation through the WAS-Exp NN model to produce a trial function $w(x, t)$ for the nPDE solution.

Step 3. Substitute the trial function into the original nPDE to convert the differential problem into an algebraic equation.

Step 4. Collect like terms in the resulting expression and set the coefficients of each basis function to zero. This yields a system of algebraic equations.

Step 5. Solve the algebraic system to determine the unknown coefficients. Substituting these back into the trial function yields a closed-form or semi-analytical solution to the original nPDE.

3. Application of WAS-Exp neural network method

In this portion, we apply the WAS-Exp neural network method on the complex hyperbolic nonlinear Schrödinger dynamical equation. We chose neural network model 3-2-1 (Figure 2) in following form:

$$\begin{aligned} \Upsilon &= F(\Upsilon_1)v_{\{1,4\}} + (F(\Upsilon_2))^2 v_{\{2,4\}} + \theta_3, \\ \Upsilon_1 &= xv_{\{1,1\}} + yv_{\{2,1\}} + tv_{\{3,1\}} + \theta_1, \\ \Upsilon_2 &= xv_{\{1,2\}} + yv_{\{2,2\}} + tv_{\{3,2\}} + \theta_2. \end{aligned} \tag{3.1}$$

Here, the first layer is the input layer consisting of x, y and t. The first hidden layer involved activation functions solution of $e^{-\psi(\Upsilon)}$ or its solutions with identity (.) and square $(.)^2$ function and the output act as a trail function of the given model represent as

$$\begin{aligned} w &= e^{-\psi(\Upsilon_1)}v_{\{1,4\}} + (e^{-\psi(\Upsilon_2)})^2 v_{\{2,4\}} + \theta_3, \\ \Upsilon_1 &= xv_{\{1,1\}} + yv_{\{2,1\}} + tv_{\{3,1\}} + \theta_1, \\ \Upsilon_2 &= xv_{\{1,2\}} + yv_{\{2,2\}} + tv_{\{3,2\}} + \theta_2. \end{aligned} \tag{3.2}$$

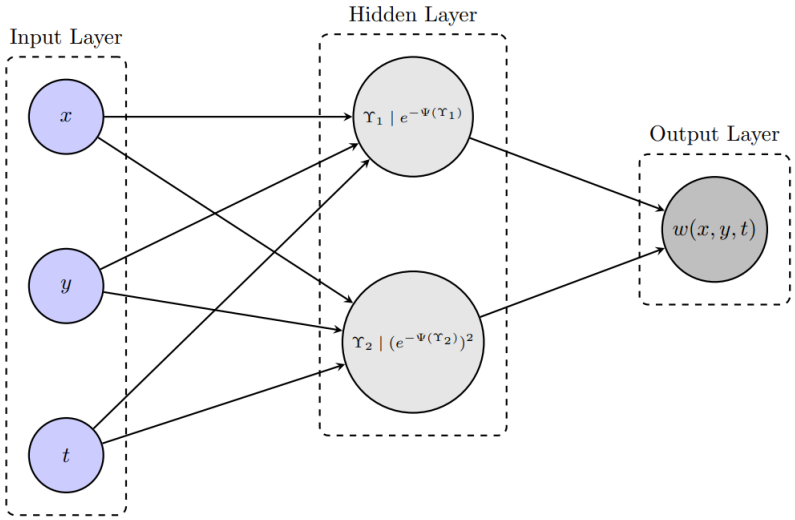

Figure 2. 3–2–1 neural network architecture. The input layer supplies the independent variables (x, y, t), the hidden neurons apply nonlinear activation functions Υ_1 and Υ_2 to perform feature extraction and the output layer yields the predicted solution $w(x, y, t)$.

By using Eq (3.2) and their respective derivatives in the concern model Eq (1.1), we got the following algebraic system:

$$
\begin{aligned}
&2\theta_3^2 v_{\{1,4\}} + 2\theta_3^2 v_{\{2,4\}} + \theta_3 v_{\{1,4\}}^2 + \theta_3 v_{\{2,4\}}^2 + 2\theta_3 v_{\{1,4\}} v_{\{2,4\}} - \beta^2 v_{\{2,4\}} v_{\{3,2\}}^2 \\
&+ \beta^2 v_{\{1,2\}}^2 v_{\{2,4\}} + 2i\beta^2 v_{\{2,2\}}^2 v_{\{2,4\}} + \theta_3^3 = 0, \\
&\alpha^2 v_{\{1,4\}} v_{\{1,1\}}^2 + 2i\alpha^2 v_{\{1,4\}} v_{\{2,1\}}^2 - \alpha^2 v_{\{1,4\}} v_{\{3,1\}}^2 = 0, \\
&3\alpha^2 v_{\{2,4\}} v_{\{1,2\}}^2 - 3\alpha^2 v_{\{2,4\}} v_{\{3,2\}}^2 + 6i\alpha^2 v_{\{2,2\}}^2 v_{\{2,4\}} = 0, \\
&2\theta_3 v_{\{1,4\}}^2 + \theta_3^2 v_{\{1,4\}} + 2\theta_3 v_{\{2,4\}} v_{\{1,4\}} + \alpha\beta v_{\{1,1\}}^2 v_{\{1,4\}} + 2i\alpha\beta v_{\{2,1\}}^2 v_{\{1,4\}} - \alpha\beta v_{\{3,1\}}^2 v_{\{1,4\}} \\
&+ v_{\{1,4\}}^3 + 2v_{\{2,4\}} v_{\{1,4\}}^2 + v_{\{2,4\}}^2 v_{\{1,4\}} = 0, \\
&2\theta_3 v_{\{2,4\}}^2 + \theta_3^2 v_{\{2,4\}} + 2\theta_3 v_{\{1,4\}} v_{\{2,4\}} + 4\alpha\beta v_{\{1,2\}}^2 v_{\{2,4\}} + 8i\alpha\beta v_{\{2,2\}}^2 v_{\{2,4\}} - 4\alpha\beta v_{\{3,2\}}^2 v_{\{2,4\}} \\
&+ v_{\{2,4\}}^3 + 2v_{\{1,4\}} v_{\{2,4\}}^2 + v_{\{1,4\}}^2 v_{\{2,4\}} = 0.
\end{aligned}
$$

After computational calculations, we get the following set of solutions.

Set 1:

$$
\left\{ v_{\{3,1\}} = -\sqrt{v_{\{1,1\}}^2 + 2iv_{\{2,1\}}^2}, v_{\{3,2\}} = -\sqrt{v_{\{1,2\}}^2 + 2iv_{\{2,2\}}^2}, v_{\{1,4\}} = -v_{\{2,4\}} - \theta_3 \right\}. \tag{3.3}
$$

Family 1.1: When $(\alpha\beta) < 0$, the solutions of hyperbolic function are

$$
\begin{aligned}
w(x, y, t) = &- \frac{\alpha v_{\{2,4\}} \tanh^2\left(\sqrt{-\alpha\beta}\left(-t\sqrt{v_{\{1,2\}}^2 + 2iv_{\{2,2\}}^2} + xv_{\{1,2\}} + yv_{\{2,2\}} + \theta_2 + Q\right)\right)}{\beta} \\
&- \sqrt{-\frac{\alpha}{\beta}}\left(v_{\{2,4\}} + \theta_3\right) \tanh\left(\sqrt{-\alpha\beta}\left(-t\sqrt{v_{\{1,1\}}^2 + 2iv_{\{2,1\}}^2} + xv_{\{1,1\}} + yv_{\{2,1\}} + \theta_1 + Q\right)\right) + \theta_3,
\end{aligned} \tag{3.4}
$$

$$w(x,y,t) = -\frac{\alpha v_{\{2,4\}} \coth^2\left(\sqrt{-\alpha\beta}\left(-t\sqrt{v_{\{1,2\}}^2 + 2iv_{\{2,2\}}^2} + xv_{\{1,2\}} + yv_{\{2,2\}} + \theta_2 + Q\right)\right)}{\beta}$$
$$- \sqrt{-\frac{\alpha}{\beta}}\left(v_{\{2,4\}} + \theta_3\right)\coth\left(\sqrt{-\alpha\beta}\left(-t\sqrt{v_{\{1,1\}}^2 + 2iv_{\{2,1\}}^2} + xv_{\{1,1\}} + yv_{\{2,1\}} + \theta_1 + Q\right)\right) + \theta_3. \tag{3.5}$$

Family 1.2: When $(\alpha\beta) > 0$, the solutions of trigonometric functions are

$$w(x,y,t) = \frac{\alpha v_{\{2,4\}} \tan^2\left(\sqrt{\alpha\beta}\left(-t\sqrt{v_{\{1,2\}}^2 + 2iv_{\{2,2\}}^2} + xv_{\{1,2\}} + yv_{\{2,2\}} + \theta_2 + Q\right)\right)}{\beta}$$
$$- \sqrt{\frac{\alpha}{\beta}}\left(v_{\{2,4\}} + \theta_3\right)\tan\left(\sqrt{\alpha\beta}\left(-t\sqrt{v_{\{1,1\}}^2 + 2iv_{\{2,1\}}^2} + xv_{\{1,1\}} + yv_{\{2,1\}} + \theta_1 + Q\right)\right) + \theta_3, \tag{3.6}$$

$$w(x,y,t) = \frac{\alpha v_{\{2,4\}} \cot^2\left(\sqrt{\alpha\beta}\left(-t\sqrt{v_{\{1,2\}}^2 + 2iv_{\{2,2\}}^2} + xv_{\{1,2\}} + yv_{\{2,2\}} + \theta_2 + Q\right)\right)}{\beta}$$
$$+ \sqrt{\frac{\alpha}{\beta}}\left(v_{\{2,4\}} + \theta_3\right)\cot\left(\sqrt{\alpha\beta}\left(-t\sqrt{v_{\{1,1\}}^2 + 2iv_{\{2,1\}}^2} + xv_{\{1,1\}} + yv_{\{2,1\}} + \theta_1 + Q\right)\right) + \theta_3. \tag{3.7}$$

Family 1.3: When $\alpha = 0$ and $\beta > 0$, the solution of rational functions is

$$w(x,y,t) = \frac{v_{\{2,4\}}}{\beta^2\left(-t\sqrt{v_{\{1,2\}}^2 + 2iv_{\{2,2\}}^2} + xv_{\{1,2\}} + yv_{\{2,2\}} + \theta_2 + Q\right)^2}$$
$$+ \frac{v_{\{2,4\}} + \theta_3}{\beta\left(-t\sqrt{v_{\{1,1\}}^2 + 2iv_{\{2,1\}}^2} + xv_{\{1,1\}} + yv_{\{2,1\}} + \theta_1 + Q\right)} + \theta_3. \tag{3.8}$$

Family 1.4: When $\alpha \neq 0$ and $\beta = 0$, the solution of rational functions is

$$w(x,y,t) = \alpha^2 v_{\{2,4\}}\left(-t\sqrt{v_{\{1,1\}}^2 + 2iv_{\{2,1\}}^2} + xv_{\{1,1\}} + yv_{\{2,1\}} + \theta_1 + Q\right)^2$$
$$- \alpha\left(v_{\{2,4\}} + \theta_3\right)\left(-t\sqrt{v_{\{1,1\}}^2 + 2iv_{\{2,1\}}^2} + xv_{\{1,1\}} + yv_{\{2,1\}} + \theta_1 + Q\right) + \theta_3. \tag{3.9}$$

Set 2:

$$\left\{v_{\{3,1\}} = \sqrt{v_{\{1,1\}}^2 + 2iv_{\{2,1\}}^2}, v_{\{1,4\}} = -\theta_3, v_{\{2,4\}} = 0\right\}. \tag{3.10}$$

Family 2.1: When $(\alpha\beta) < 0$, the solutions of hyperbolic function are

$$w(x,y,t) = \theta_3\left(1 - \sqrt{-\frac{\alpha}{\beta}}\tanh\left(\sqrt{-\alpha\beta}\left(t\sqrt{v_{\{1,1\}}^2 + 2iv_{\{2,1\}}^2} + xv_{\{1,1\}} + yv_{\{2,1\}} + \theta_1 + Q\right)\right)\right), \tag{3.11}$$

$$w(x,y,t) = \theta_3\left(1 - \sqrt{-\frac{\alpha}{\beta}}\coth\left(\sqrt{-\alpha\beta}\left(t\sqrt{v_{\{1,1\}}^2 + 2iv_{\{2,1\}}^2} + xv_{\{1,1\}} + yv_{\{2,1\}} + \theta_1 + Q\right)\right)\right). \tag{3.12}$$

Family 2.2: When $(\alpha\beta) > 0$, the solutions of trigonometric functions are

$$w(x,y,t) = \theta_3\left(1 - \sqrt{\frac{\alpha}{\beta}}\tan\left(\sqrt{\alpha\beta}\left(t\sqrt{v_{\{1,1\}}^2 + 2iv_{\{2,1\}}^2} + xv_{\{1,1\}} + yv_{\{2,1\}} + \theta_1 + Q\right)\right)\right), \tag{3.13}$$

$$w(x,y,t)=\theta_3\left(1+\sqrt{\frac{\alpha}{\beta}}\cot\left(\sqrt{\alpha\beta}\left(t\sqrt{v_{\{1,1\}}^2+2iv_{\{2,1\}}^2}+xv_{\{1,1\}}+yv_{\{2,1\}}+\theta_1+Q\right)\right)\right). \tag{3.14}$$

Family 2.3: When $\alpha=0$ and $\beta>0$, the solution of rational functions is

$$w(x,y,t)=\theta_3\left(1+\frac{1}{\beta\left(t\sqrt{v_{\{1,1\}}^2+2iv_{\{2,1\}}^2}+xv_{\{1,1\}}+yv_{\{2,1\}}+\theta_1+Q\right)}\right). \tag{3.15}$$

Family 2.4: When $\alpha\neq 0$ and $\beta=0$, the solution of rational functions is

$$w(x,y,t)=\theta_3\left(1-\alpha\left(t\sqrt{v_{\{1,1\}}^2+2iv_{\{2,1\}}^2}+xv_{\{1,1\}}+yv_{\{2,1\}}+\theta_1+Q\right)\right). \tag{3.16}$$

Set 3:

$$\left\{v_{\{3,2\}}=\sqrt{v_{\{1,2\}}^2+2iv_{\{2,2\}}^2},v_{\{1,4\}}=0,v_{\{2,4\}}=-\theta_4\right\}. \tag{3.17}$$

Family 3.1: When $(\alpha\beta)<0$, the solutions of hyperbolic function are

$$w(x,y,t)=\frac{\theta_3\left(\beta+\alpha\tanh^2\left(\sqrt{-\alpha\beta}\left(t\sqrt{v_{\{1,2\}}^2+2iv_{\{2,2\}}^2}+xv_{\{1,2\}}+yv_{\{2,2\}}+\theta_2+Q\right)\right)\right)}{\beta}, \tag{3.18}$$

$$w(x,y,t)=\frac{\theta_3\left(\beta+\alpha\coth^2\left(\sqrt{-\alpha\beta}\left(t\sqrt{v_{\{1,2\}}^2+2iv_{\{2,2\}}^2}+xv_{\{1,2\}}+yv_{\{2,2\}}+\theta_2+Q\right)\right)\right)}{\beta}. \tag{3.19}$$

Family 3.2: When $(\alpha\beta)>0$, the solutions of trigonometric functions are

$$w(x,y,t)=\frac{\theta_3\left(\beta-\alpha\tan^2\left(\sqrt{\alpha\beta}\left(t\sqrt{v_{\{1,2\}}^2+2iv_{\{2,2\}}^2}+xv_{\{1,2\}}+yv_{\{2,2\}}+\theta_2+Q\right)\right)\right)}{\beta}, \tag{3.20}$$

$$w(x,y,t)=\frac{\theta_3\left(\beta-\alpha\cot^2\left(\sqrt{\alpha\beta}\left(t\sqrt{v_{\{1,2\}}^2+2iv_{\{2,2\}}^2}+xv_{\{1,2\}}+yv_{\{2,2\}}+\theta_2+Q\right)\right)\right)}{\beta}. \tag{3.21}$$

Family 3.3: When $\alpha=0$ and $\beta>0$, the solution of rational functions is

$$w(x,y,t)=\theta_3\left(1-\frac{1}{\beta^2\left(t\sqrt{v_{\{1,2\}}^2+2iv_{\{2,2\}}^2}+xv_{\{1,2\}}+yv_{\{2,2\}}+\theta_2+Q\right)^2}\right). \tag{3.22}$$

Family 3.4: When $\alpha\neq 0$ and $\beta=0$, the solution of rational functions is

$$w(x,y,t)=\theta_3\left(1-\alpha^2\left(tv_{\{3,1\}}+xv_{\{1,1\}}+yv_{\{2,1\}}+\theta_1+Q\right)^2\right). \tag{3.23}$$

Verification: To ensure the correctness of the obtained solutions, we substitute each solution back into the governing equation (1.1) and verify that it is satisfied identically. For instance, for the solution $w(x,y,t)$ given in (3.4) and their respective derivatives w_{yy}, w_{xx} and w_{tt}, we have

$$\text{LHS of (1.1)}=iw_{yy}+\frac{1}{2}\left(w_{xx}-w_{tt}\right)+|w|^2w=0,$$

which confirms that the solution satisfies the governing equation exactly. Similar checks have been performed for all other solutions presented in this section.

4. Wave dynamic profile

Wave profile discussion is an important part in the study of the soliton solutions. Here, we discuss the wave profile of our gained soliton solutions in different forms.

We discuss soliton solutions with Abs(w), Re(w), and Im(w) values. The plot shows kink type solutions in 3D and 2D surfaces for the Abs(w) in orange, Re(w) in blue, and Im(w) in green shade of solution equation (3.11) in Figure 3 with $v_{\{1,1\}} = 0.5$, $v_{\{2,1\}} = 0.2$, $\theta_1 = -1$, $\theta_3 = 0.5$, $t = 1$, $Q = 0.3$, $\alpha = 0.3$, and $\beta = -0.2$.

The plot shows bright type solutions in 3D and 2D surfaces for the Abs(w) in orange, Re(w) in blue, and Im(w) in green shade of solution equation (3.12) in Figure 4 with $v_{\{1,1\}} = 1.5$, $v_{\{2,1\}} = 1.2$, $\theta_1 = -1$, $\theta_3 = 0.5$, $t = 1$, $Q = 0.3$, $\alpha = 0.3$, and $\beta = -0.2$.

The plot shows periodic type solutions in 3D and 2D surfaces for the Abs(w) in orange, Re(w) in blue, and Im(w) in green shade of solution equation (3.13) in Figure 5 with $v_{\{1,1\}} = 1.5$, $v_{\{2,1\}} = 1.2$, $\theta_1 = 1$, $\theta_3 = 0.5$, $t = 1$, $Q = 0.3$, $\alpha = 0.3$, and $\beta = 0.2$.

The plot shows bright-periodic type solutions in 3D and 2D surfaces for the Abs(w) in orange, Re(w) in blue, and Im(w) in green shade of solution equation (3.14) in Figure 6 with $v_{\{1,1\}} = 1.5$, $v_{\{2,1\}} = 1.2$, $\theta_1 = 1$, $\theta_3 = 0.5$, $t = 1$, $Q = 0.3$, $\alpha = 0.3$, and $\beta = 0.2$.

The plot shows breather type solutions in 3D and 2D surfaces for the Abs(w) in orange, Re(w) in blue, and Im(w) in green shade of solution equation (3.16) in Figure 7 with $v_{\{1,1\}} = 1.5$, $v_{\{2,1\}} = 1.2$, $\theta_1 = 1$, $\theta_3 = 0.5$, $t = 1$, $Q = 0.3$, and $\alpha = 0.3$.

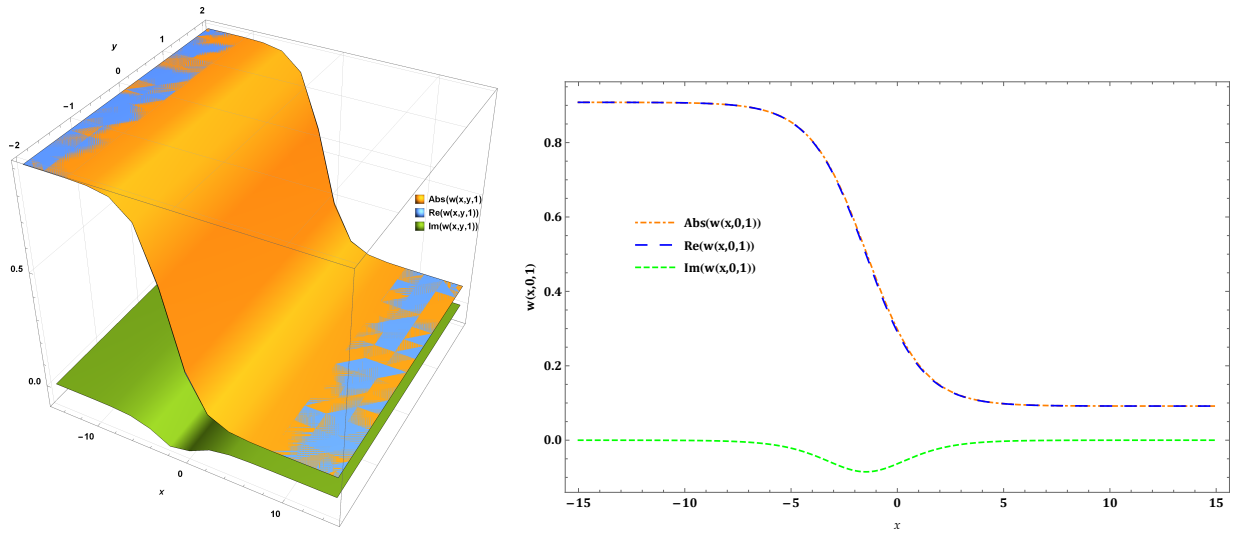

(a) (b)

Figure 3. The plot shows kink type solutions in 3D and 2D surfaces for the Abs(w) in orange, Re(w) in blue, and Im(w) in green shade solution appear in Eq (3.11).

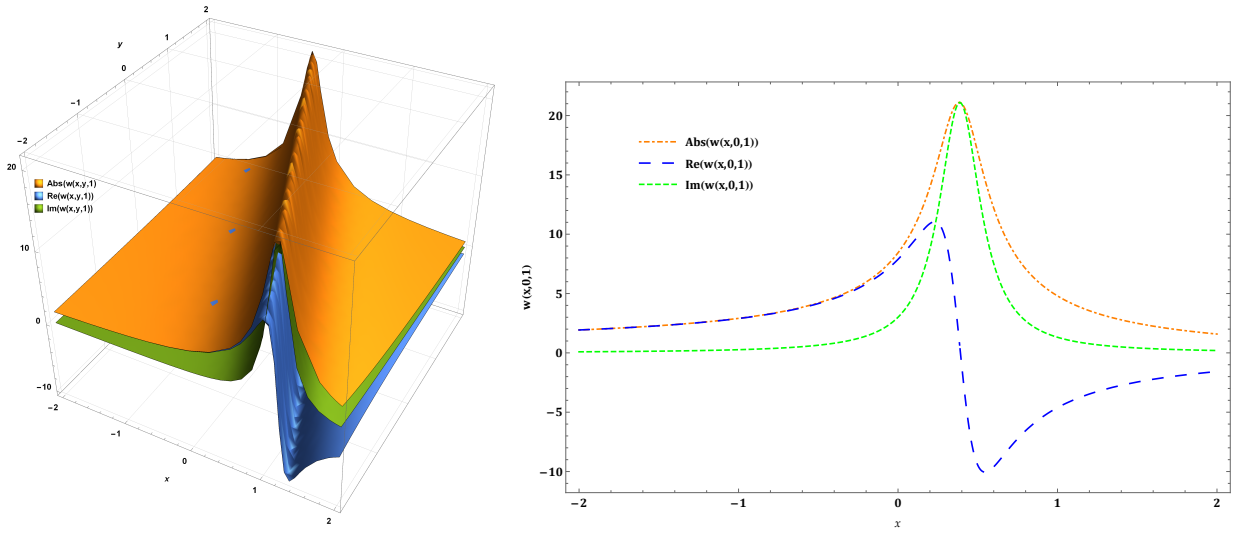

(a) (b)

Figure 4. The plot shows bright type solutions in 3D and 2D surfaces for the Abs(w) in orange, Re(w) in blue, and Im(w) in green shade solution appear in Eq (3.12).

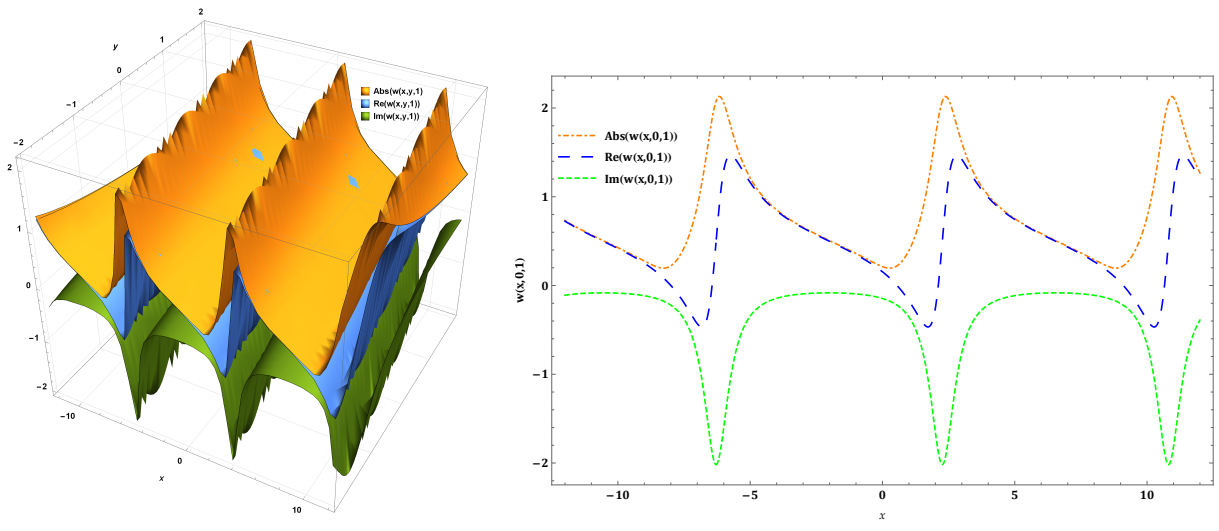

(a) (b)

Figure 5. The plot shows periodic type solutions in 3D and 2D surfaces for the Abs(w) in orange, Re(w) in blue, and Im(w) in green shade solution appear in Eq (3.13).

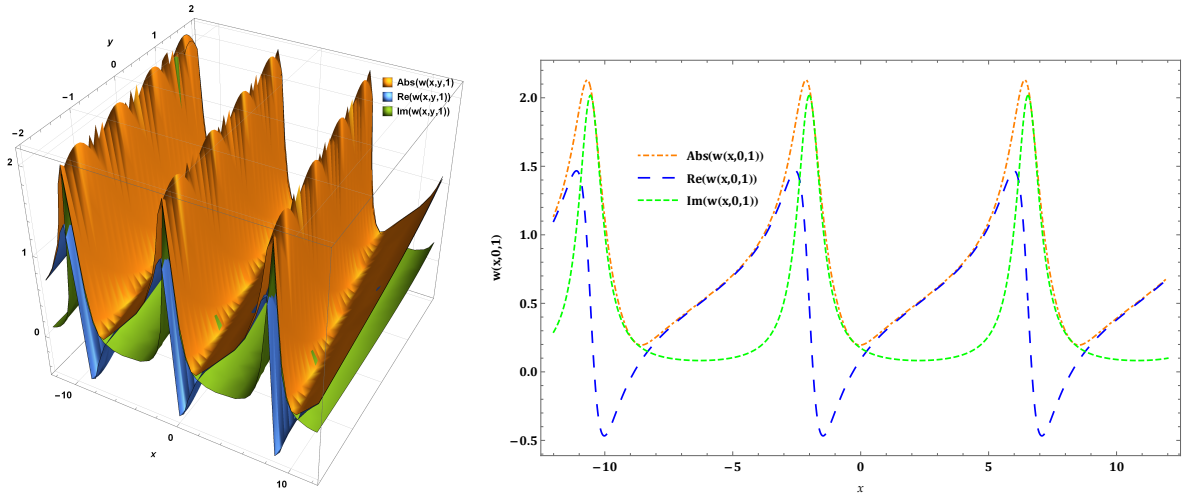

(a) (b)

Figure 6. The plot shows bright-periodic type solutions in 3D and 2D surfaces for the Abs(w) in orange, Re(w) in blue, and Im(w) in green shade solution appear in Eq (3.14).

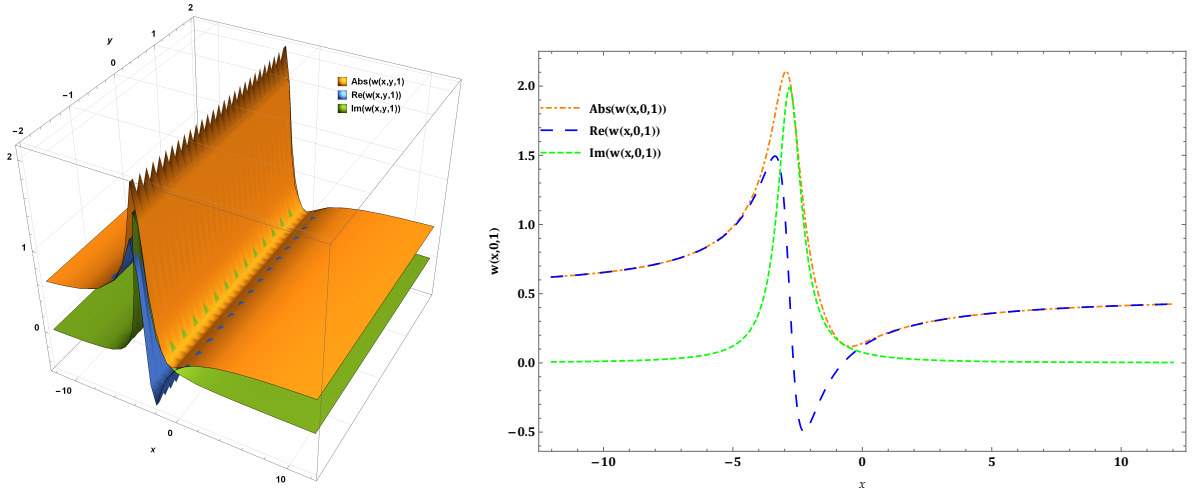

(a) (b)

Figure 7. The plot shows breather type solutions in 3D and 2D surfaces for the Abs(w) in orange, Re(w) in blue, and Im(w) in green shade solution appear in Eq (3.15).

To highlight the novelty of our wave profiles, we compare them with known results for related nonlinear evolution equations. Traditional studies usually report standard bright, dark, periodic, or kink-type waves with fixed amplitude-width relations. In contrast, the present solutions exhibit a richer set of profiles arising from the free parameters $v_{i,j}$, θ_k, and the nonlinear coupling of the hyperbolic functions. This flexibility allows independent control of amplitude, steepness and localization, and also produces mixed-profile structures that have not been reported for this class of equations. These features demonstrate that our results extend existing solution families and introduce genuinely new wave behaviours.

4.1. Results and discussion

This section is about the discussion of the WAS-Exp NN method and the other analytical methods. Table 1 shows the some advantages of the other analytical method of the WAS-Exp NN method.

Table 1. Advantages.

Method	The WAS-Exp NN method	Other analytical methods
Solve all nonlinear and complex partial differential equations	Yes (All)	No (Only limited)
Use travelling wave transformation to reduce the PDE into ODE	No	Yes
No, of calculations	Less	More
By adjusting the hidden layers to overcome complexity	Yes	No
Need balance method to suppose finite series solution	No	Yes

Unlike conventional analytical and hybrid methods, which typically require similarity transformations or travelling wave reductions to convert the governing PDEs and ODEs, the WAS-Exp neural network method operates directly on the original partial differential equations. This eliminates restrictive assumptions on solution structure and allows greater flexibility in capturing complex nonlinear dynamics. Moreover, the proposed approach integrates analytical structure with data-driven learning, providing stable, accurate, and computationally efficient solutions for nonlinear PDEs.

5. Machine learning analysis

This portion executes the machine learning analysis through the multi-layer perceptron regressor algorithm [30, 31]. Through this algorithm we predict the behavior of the gained solution and compare with actual solutions in Figure 8–12 and the losses in the Table 2–6. We found the prediction of this algorithm was close to our actual solutions wave behavior.

- **Data split:** 80% training and 20% testing
- **Normalization range:** [0, 1]
- **Neural network structure:** Input and output layers with multiple hidden layers
- **Propagation method:** Forward and backward propagation
- **Activation function:** Sigmoid
- **Optimization algorithm:** Gradient descent
- **Loss function:** Mean squared error (MSE)
- **Learning rate:** 0.1
- **Training iterations:** Between 1000 and 50,000 epochs
- **Implementation tool:** Python 3.13.1
- **Outputs:** Actual vs. predicted plots and loss convergence

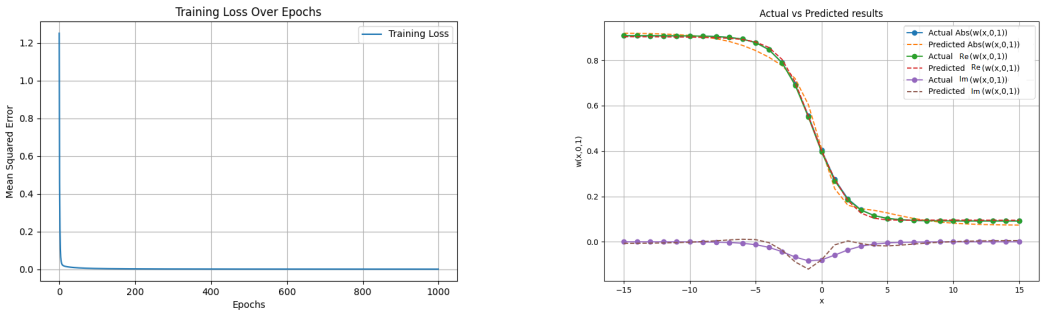

(a) (b)

Figure 8. This plot shows kink type solution prediction with loss in (a), 2D surface in (b) for the Abs(w) in orange, Re(w) in red, and Im(w) in brown dashed line solution appear in Eq (3.11).

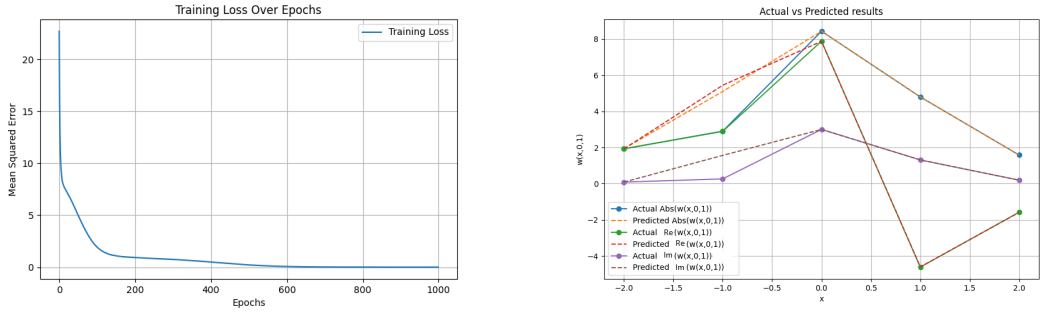

(a) (b)

Figure 9. This plot shows bright type solution prediction with loss in (a), 2D surface in (b) for the Abs(w) in orange, Re(w) in red and Im(w) in brown dashed line solution appear in Eq (3.12).

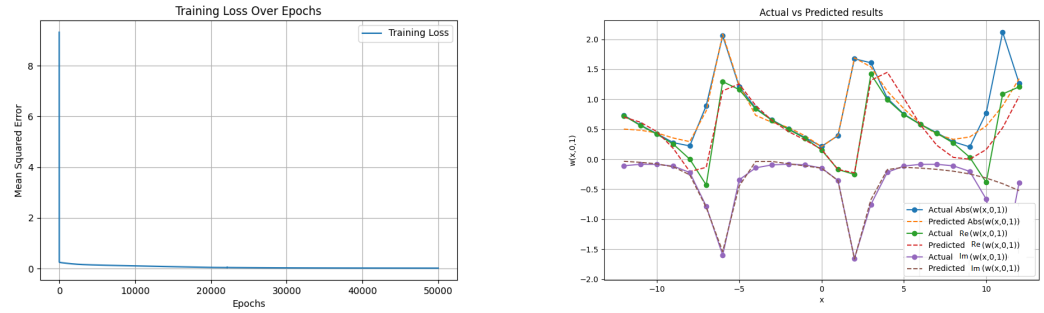

(a) (b)

Figure 10. This plot shows periodic type solution prediction with loss in (a), 2D surface in (b) for the Abs(w) in orange, Re(w) in red, and Im(w) in brown dashed line solution appear in Eq (3.13).

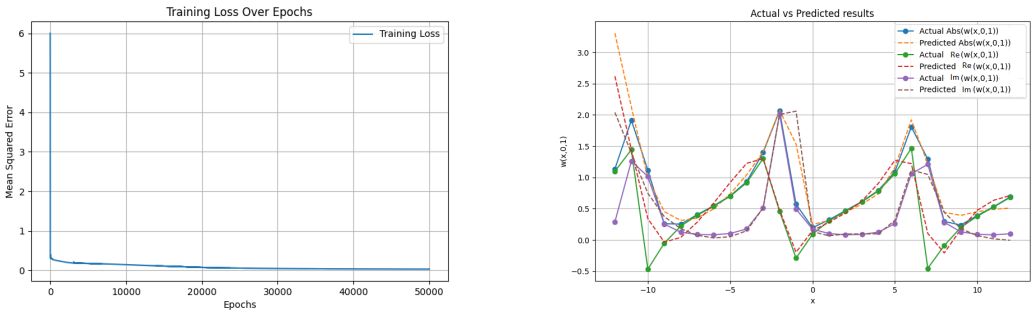

(a) (b)

Figure 11. This plot shows bright-periodic type solution prediction with loss in (a), 2D surface in (b) for the Abs(w) in orange, Re(w) in red, and Im(w) in brown dashed line solution appear in Eq (3.14).

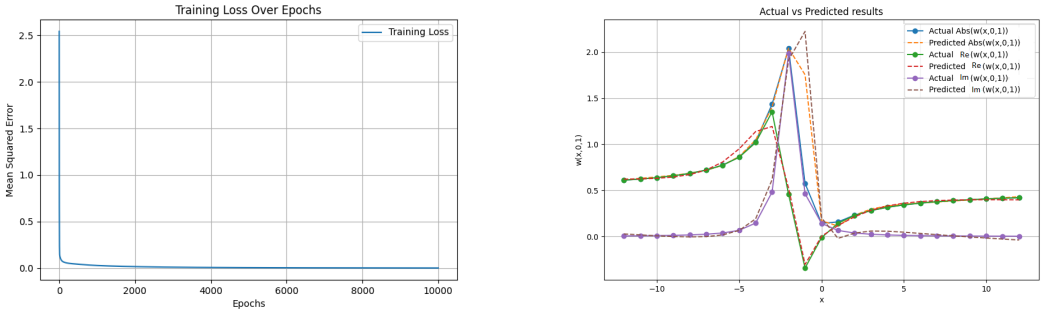

(a) (b)

Figure 12. This plot shows breather type solution prediction with loss in (a), 2D surface in (b) for the Abs(w) in orange, Re(w) in red, and Im(w) in brown dashed line solution appear in Eq (3.15).

Table 2. Loss values show the performance during the machine learning prediction of solution equation (3.11).

Epoch	Loss	Epoch	Loss
100	3.0642	600	0.1003
200	0.9314	700	0.0311
300	0.6948	800	0.0090
400	0.4898	900	0.0026
500	0.2606	1000	0.0008

Table 3. Loss values show the performance during the machine learning prediction of solution equation (3.12).

Epoch	Loss	Epoch	Loss
100	0.0036	600	0.0005
200	0.0017	700	0.0004
300	0.0010	800	0.0003
400	0.0007	900	0.0003
500	0.0006	1000	0.0002

Table 4. Loss values shows the performance during the machine learning prediction of solution equation (3.13).

Epoch	Loss	Epoch	Loss
5000	0.1699	30000	0.0424
10000	0.1406	35000	0.0364
15000	0.1049	40000	0.0324
20000	0.0710	45000	0.0295
25000	0.0529	50000	0.0272

Table 5. Loss values show the performance during the machine learning prediction of solution equation (3.14).

Epoch	Loss	Epoch	Loss
5000	0.1384	30000	0.0268
10000	0.1063	35000	0.0226
15000	0.0733	40000	0.0199
20000	0.0453	45000	0.0180
25000	0.0346	50000	0.0167

Table 6. Loss values show the performance during the machine learning prediction of solution equation (3.15).

Epoch	Loss	Epoch	Loss
1000	0.0284	6000	0.0040
2000	0.0160	7000	0.0031
3000	0.0105	8000	0.0024
4000	0.0074	9000	0.0019
5000	0.0054	10000	0.0015

6. Asymptotic analysis of solutions

Asymptotic analysis is essential for understanding the far-field behavior of nonlinear wave solutions. It identifies constant end states, ensures solution boundedness, and confirms physical

stability. Moreover, it provides a theoretical benchmark for validating numerical and machine learning-based approximations. In this section, we apply the asymptotic analysis on acquire solutions. So first we apply on Eq (3.11). For x-asymptotic $v_{\{1,1\}} = 0.5$, $v_{\{2,1\}} = 0.2$, $\theta_1 = -1$, $\theta_3 = 0.5$, $t = 0$, $Q = 0.3$, $\alpha = 0.3, \beta = -0.2$, $y = 0$, for t-asymptotic $v_{\{1,1\}} = 0.2$, $v_{\{2,1\}} = 0.2$, $\theta_1 = -1.1$, $\theta_3 = 0.5$, $y = 0$, $Q = 1$, $\lambda = 1.3, \mu = -0.1$, $x = 0$, for y-asymptotic $v_{\{1,1\}} = 0.5$, $v_{\{2,1\}} = 1.2$, $\theta_1 = -1$, $\theta_3 = 0.5$, $t = 0$, $Q = 0.3$, $\lambda = 0.3, \mu = -0.2$, $x = 0$.

Case 1: If $x \to \pm\infty$ at $y, t = 0$,

$$w(x,0,0) = \theta_3\left(1 - \sqrt{-\frac{\alpha}{\beta}}\tanh\left(\sqrt{-\alpha\beta}\,(xv_{\{1,1\}} + \theta_1 + Q)\right)\right). \tag{6.1}$$

The asymptotic behavior of the obtained solutions is derived directly from their explicit functional forms. By applying the limiting property

$$\tanh(x) \to \pm 1 \quad \text{as} \quad x \to \pm\infty,$$

it follows that the solutions approach constant end states at spatial infinity. This behavior confirms the localized nature of the solutions and indicates their physical stability.

Case 2: If $t \to \pm\infty$ at $x, y = 0$,

$$w(0,0,t) = \theta_3\left(1 - \sqrt{-\frac{\alpha}{\beta}}\tanh\left(\sqrt{-\alpha\beta}\left(t\sqrt{v_{\{1,1\}}^2 + 2iv_{\{2,1\}}^2} + \theta_1 + Q\right)\right)\right). \tag{6.2}$$

Case 3: If $y \to \pm\infty$ at $x, t = 0$,

$$w(0,y,0) = \theta_3\left(1 - \sqrt{-\frac{\alpha}{\beta}}\tanh\left(\sqrt{-\alpha\beta}\,(yv_{\{2,1\}} + \theta_1 + Q)\right)\right). \tag{6.3}$$

Figures 13, 14, and 15 below show the asymptotic behavior of the Eqs (6.1), (6.2) and (6.3), respectively.

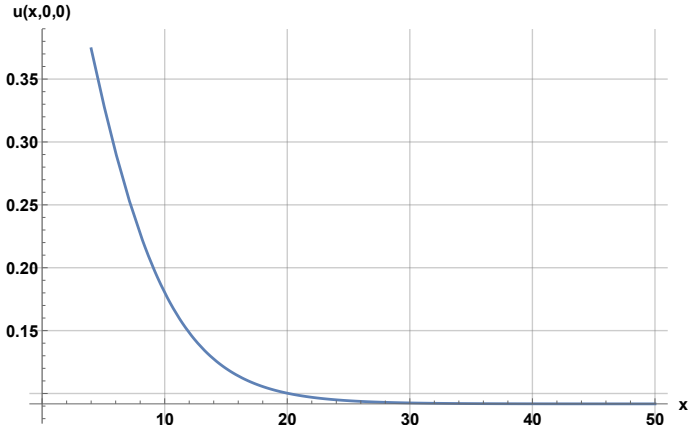

Figure 13. x-asymptotic behavior of Eq (6.1).

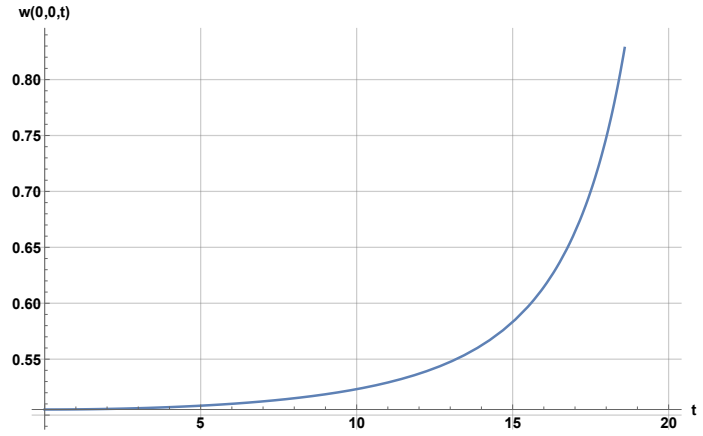

Figure 14. t-asymptotic behavior of Eq (6.2).

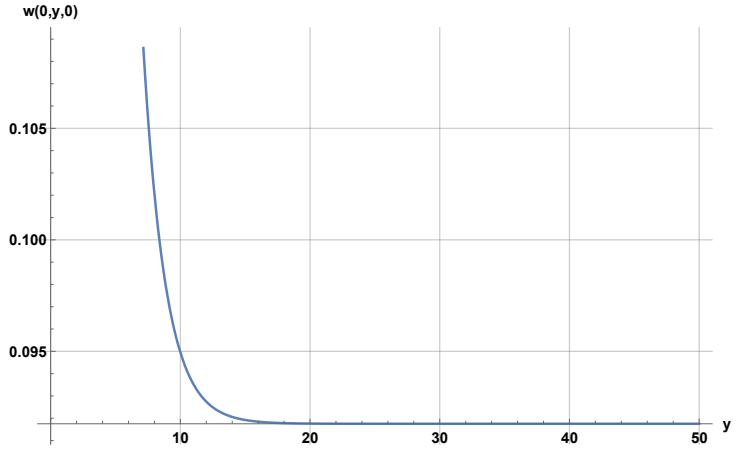

Figure 15. y-asymptotic behavior of Eq (6.3).

Now we apply on the solution equation (3.15), for x-asymptotic $t = 0$ and $y = 0$, for t-asymptotic $y = 0$ and $x = 0$, for y-asymptotic $x = 0$ and $t = 0$ with $v_{\{1,1\}} = 1.5$, $v_{\{2,1\}} = 1.2$, $\theta_1 = -2$, $\theta_3 = 1$, $Q = 0.3$, $\alpha = 0.1$.

Case 1: If $x \to \pm\infty$ at $y, t = 0$,

$$w(x, 0, 0) = \theta_3 \left(1 + \frac{1}{\beta\left(x v_{\{1,1\}} + \theta_1 + Q\right)}\right). \tag{6.4}$$

Case 2: If $t \to \pm\infty$ at $x, y = 0$,

$$w(0, 0, t) = \theta_3 \left(1 + \frac{1}{\beta\left(t\sqrt{v_{\{1,1\}}^2 + 2iv_{\{2,1\}}^2} + \theta_1 + Q\right)}\right). \tag{6.5}$$

Case 3: If $y \to \pm\infty$ at $x, t = 0$,

$$w(0, y, 0) = \theta_3 \left(1 + \frac{1}{\beta\left(y v_{\{2,1\}} + \theta_1 + Q\right)}\right). \tag{6.6}$$

Figures 16, 17, and 18 below show the asymptotic behavior of the Eqs (6.4), (6.5), and (6.6), respectively. Similarly, we can check asymptotic behavior of the other solutions. Physically, the asymptotic states correspond to stable background wave levels, indicating that the localized structures propagate without distortion and maintain their integrity over long distances.

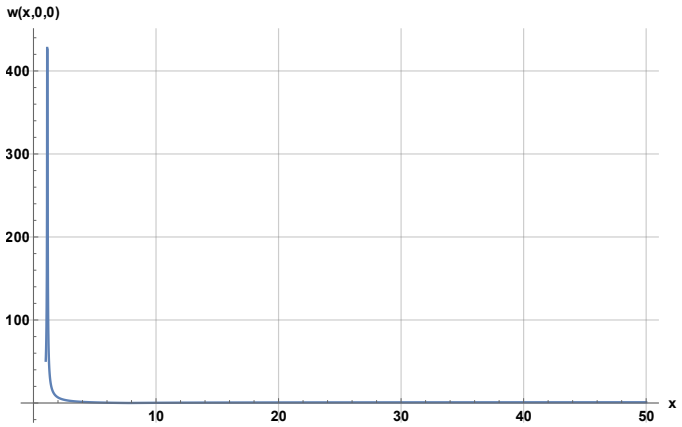

Figure 16. x-asymptotic behavior of Eq (6.4).

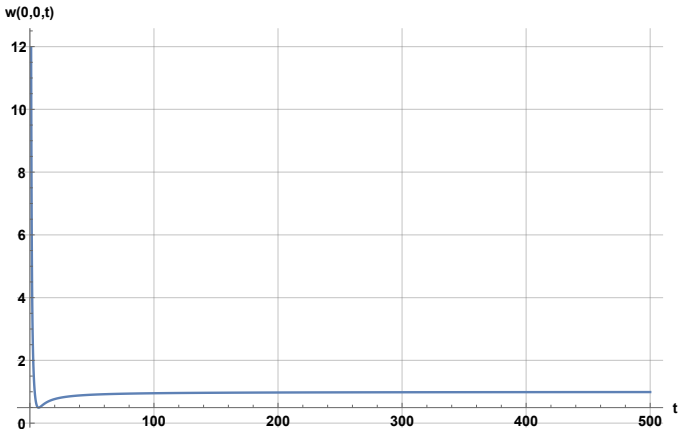

Figure 17. t-asymptotic behavior of Eq (6.5).

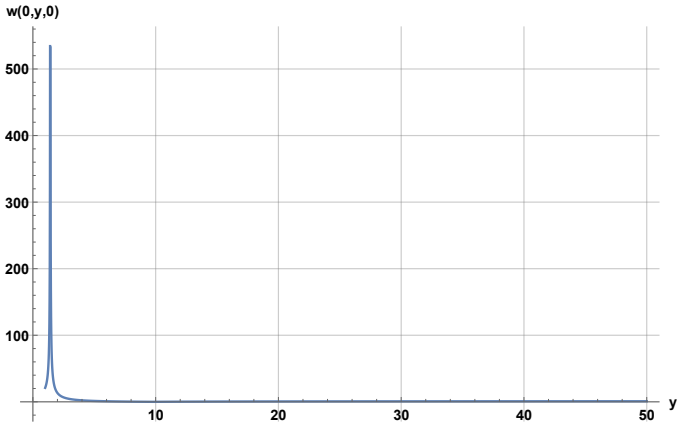

Figure 18. y-asymptotic behavior of Eq (6.6).

7. Conclusions

In this work, the CHNLSDE was successfully solved by using a newly proposed WAS-Exp neural network method. The approach made it possible to systematically derive exact analytical solutions that included the combined effects of dispersion and nonlinearity. These solutions included bright, kink solitary, periodic and bright-periodic wave profiles. The physical behavior of these solutions is further demonstrated by the graphical analysis in 3D and 2D. The obtained solution families possess direct practical significance: Bright and periodic waves model energy localization and signal stability in nonlinear optical fibers, while kink-type structures describe transition layers and ion-acoustic disturbances in plasma environments. These analytical profiles can therefore be used to predict wave propagation, stability thresholds, and modulation patterns in real physical systems. Such applications underscore the usefulness of the derived solutions for designing and analyzing wave-based technologies in plasma physics, optical communication, and other nonlinear media. In addition to expanding the collection of known solutions for nonlinear models, this work offers a helpful framework for examining related equations in further investigations. Furthermore, machine learning analysis executed on the obtained solution for examine the wave dynamic behavior of the actual and predict outcomes. Lastly, we plot the x-asymptotic, y-asymptotic and t-asymptotic behavior of the gained solutions through the 2D surfaces.

Author contributions

W. Razzaq, A. Zafar, A. Al Nuaim and N. Almusallam: Concept, Methodology, Investigation, Formal analysis, Visualization, Writing–review and editing. All authors have read and approved the final version of the manuscript for publication.

Use of Generative-AI tools declaration

The authors declare they have not used Artificial Intelligence (AI) tools in the creation of this article.

Funding

This work was supported by the Deanship of Scientific Research, Vice Presidency for Graduate Studies and Scientific Research, King Faisal University, Saudi Arabia [KFU254743].

Conflict of interest

All authors declare no conflicts of interest in this paper.

References

1. British Association for the Advancement of Science, *Report of the annual meeting*, 1845.
2. P. G. Drazin, R. S. Johnson, *Solitons: an introduction*, Cambridge University Press, 1989.

3. P. R. Kundu, M. R. A. Fahim, M. E. Islam, M. A. Akbar, The sine-Gordon expansion method for higher-dimensional NLEEs and parametric analysis, *Heliyon*, **7** (2021), e06458. https://doi.org/10.1016/j.heliyon.2021.e06459
4. A. Irshad, N. Ahmed, U. Khan, S. T. Mohyud-Din, I. Khan, E. S. M. Sherif, Optical solutions of Schrödinger equation using extended sinh-Gordon equation expansion method, *Front. Phys.*, **8** (2020), 73. https://doi.org/10.3389/fphy.2020.00073
5. M. Ozisik, A. Secer, M. Bayram, Obtaining analytical solutions of (2+1)-dimensional nonlinear Zoomeron equation by using modified F-expansion and modified generalized Kudryashov methods, *Eng. Comput.*, **41** (2024), 1105–1120. https://doi.org/10.1108/EC-10-2023-0688
6. P. F. Han, T. Bao, Novel hybrid-type solutions for the (3+1)-dimensional generalized Bogoyavlensky-Konopelchenko equation with time-dependent coefficients, *Nonlinear Dyn.*, **107** (2022), 1163–1177. https://doi.org/10.1007/s11071-021-07019-5
7. S. Kumar, S. Rani, Symmetries of optimal system, various closed-form solutions, and propagation of different wave profiles for the Boussinesq-Burgers system in ocean waves, *Phys. Fluids*, **34** (2022), 037109. https://doi.org/10.1063/5.0085927
8. A. M. Wazwaz, Extended (3+1)-dimensional Kairat-II and Kairat-X equations: Painlevé integrability, multiple soliton solutions, lump solutions, and breather wave solutions, *Int. J. Numer. Methods Heat Fluid Flow*, **34** (2024), 2177–2194. https://doi.org/10.1108/HFF-01-2024-0053
9. A. Yokus, M. Yavuz, Novel comparison of numerical and analytical methods for fractional Burger-Fisher equation, *Discrete Contin. Dyn. Syst. Ser. S*, **14** (2021), 2591–2606. https://doi.org/10.3934/dcdss.2020258
10. Y. Pandir, A. Ekin, New solitary wave solutions of the Korteweg-de Vries (KdV) equation by new version of the trial equation method, *Electron. J. Appl. Math.*, **1** (2023), 101–113. https://doi.org/10.61383/ejam.20231130
11. A. R. Alharbi, M. B. Almatrafi, M. A. E. Abdelrahman, Analytical and numerical investigation for Kadomtsev-Petviashvili equation arising in plasma physics, *Phys. Scr.*, **95** (2020), 045215. https://doi.org/10.1088/1402-4896/ab6ce4
12. A. Khan, S. Saifullah, S. Ahmad, M. A. Khan, M. ur Rahman, Dynamical properties and new optical soliton solutions of a generalized nonlinear Schrödinger equation, *Eur. Phys. J. Plus*, **138** (2023), 1059. https://doi.org/10.1140/epjp/s13360-023-04697-5
13. A. Zafar, M. Shakeel, A. Ali, H. Rezazadeh, A. Bekir, Analytical study of complex Ginzburg-Landau equation arising in nonlinear optics, *J. Nonlinear Opt. Phys. Mater.*, **32** (2023), 2350010. https://doi.org/10.1142/S0218863523500108
14. A. Zafar, W. Razzaq, H. Rezazadeh, M. Eslami, The complex hyperbolic Schrödinger dynamical equation with a truncated M-fractional by using simplest equation method, *Comput. Methods Differ. Equ.*, **12** (2024), 44–55. https://doi.org/10.22034/cmde.2022.40084.1747
15. W. O. Apeanti, A. R. Seadawy, D. C. Lu, Complex optical solutions and modulation instability of hyperbolic Schrödinger dynamical equation, *Results Phys.*, **12** (2019), 2091–2097. https://doi.org/10.1016/j.rinp.2019.02.014

16. S. Correia, M. Figueira, The hyperbolic nonlinear Schrödinger equation, 2015, arXiv: 1510.08745V1.

17. M. A. Bakar, S. Owyed, W. A. Faridi, M. A. El-Rahman, M. Sallah, The first integral of the dissipative nonlinear Schrödinger equation with Nucci's direct method and explicit wave profile formation, *Fractal Fract.*, **7** (2023), 1–18. https://doi.org/10.3390/fractalfract7010038

18. V. Kumar, R. Jiwari, A. R. Djurayevich, M. U. Khudoyberganov, Hyperbolic (3+1)-dimensional nonlinear Schrödinger equation: Lie symmetry analysis and modulation instability, *J. Math.*, **2022** (2022), 9050272. https://doi.org/10.1155/2022/9050272

19. S. Akram, M. ur Rahman, L. A. Al-Essa, Lump-breather interactions and inelastic wave dynamics in KdV hierarchy systems via the bilinear neural network-based approach, *Int. J. Theor. Phys.*, **64** (2025), 1–15. https://doi.org/10.1007/s10773-025-06173-5

20. D. Baleanu, K. Hosseini, S. Salahshour, K. Sadri, M. Mirzazadeh, C. Park, et al., The (2+1)-dimensional hyperbolic nonlinear Schrödinger equation and its optical solitons, *AIMS Math.*, **6** (2021), 9568–9581. https://doi.org/ 10.3934/math.2021556

21. D. Sherriffe, D. Behera, P. Nagarani, Different forms for exact traveling wave solutions of unstable and hyperbolic nonlinear Schrödinger equations, *Int. J. Mod. Phys. B*, **38** (2024), 2450131. https://doi.org/10.1142/S0217979224501315

22. S. Kumar, A. Kukkar, Dynamics of several optical soliton solutions of a (3+1)-dimensional nonlinear Schrödinger equation with parabolic law in optical fibers, *Mod. Phys. Lett. B*, **39** (2025), 2450453. https://doi.org/10.1142/S0217984924504530

23. M. M. Rahman, A. Aktar, K. C. Roy, Analytical solutions of nonlinear coupled Schrödinger-KdV equation via advance exponential expansion, *Amer. J. Math. Comput. Model.*, **3** (2018), 46–51. https://doi.org/10.11648/j.ajmcm.20180303.11

24. A. Ghaffar, A. Ali, S. Ahmed, S. Akram, M. U. D. Junjua, D. Baleanu, et al., A novel analytical technique to obtain the solitary solutions for nonlinear evolution equation of fractional order, *Adv. Differ. Equ.*, **2020** (2020), 308. https://doi.org/10.1186/s13662-020-02751-5

25. S. Ahmed, B. S. T. Alkahtani, S. S. Alzaid, Wave propagation and soliton behaviors for the strain equation by using the sub-ODE method and expansion technique, *Int. J. Appl. Comput. Math.*, **10** (2024), 122. https://doi.org/10.1007/s40819-024-01761-1

26. A. Ciancio, H. M. Baskonus, T. A. Sulaiman, H. Bulut, New structural dynamics of isolated waves via the coupled nonlinear Maccari's system with complex structure, *Indian J. Phys.*, **92** (2018), 1281–1290. https://doi.org/10.1007/s12648-018-1204-6

27. E. Hussain, Z. Li, S. A. A. Shah, E. A. Az-Zo'bi, M. Hussien, Dynamics study of stability analysis, sensitivity insights and precise soliton solutions of the nonlinear (STO)-Burger equation, *Opt. Quantum Electron.*, **55** (2023), 1274. https://doi.org/10.1007/s11082-023-05588-w

28. A. Fahad, H. Ur Rehman, I. Iqbal, Y. H. Qian, M. S. Saleem, Optimizing space curve motion in Kuralay model through diverse soliton approaches, *Opt. Quantum Electron.*, **56** (2024), 788. https://doi.org/10.1007/s11082-024-06568-4

29. W. B. Ma, S. Bilige, Novel interaction solutions to the (3+1)-dimensional Hirota bilinear equation by bilinear neural network method, *Mod. Phys. Lett. B*, **38** (2024), 2450240. https://doi.org/10.1142/S0217984924502403

30. W. Razzaq, A. Zafar, Bilinearization of generalized Bogoyavlensky-Konopelchenko equation for solitons with neural networks: Painleve analysis, *Nonlinear Dyn.*, **113** (2025), 25083–25096. https://doi.org/10.1007/s11071-025-11384-w

31. W. Razzaq, A. Zafar, Machine learning-enhanced soliton solutions for the Lonngren-wave equation: an integration of Painlevé analysis and Hirota bilinear method, *Rend. Lincei Sci. Fis. Nat.*, **36** (2025), 917–932. https://doi.org/10.1007/s12210-025-01354-0

AIMS Press